

SIMULATING A POSITRON CONVERTER IN BMAD

John Mastroberti, Indiana University, Bloomington, IN, 47405, USA
David Sagan and Jim Shanks, Cornell University, Ithaca, NY, 14850, USA

Abstract

A model to describe the output particle distribution generated by particles impinging on a planar target has been developed. This model was developed to simulate positron production in the Cornell CESR Linac but can be applied to targets using different types of particles.

To model a specific converter target, the output particle distribution is first simulated by tracking particles using the Geant4 toolkit which models the fundamental physics of the conversion process. The Monte Carlo distribution from Geant4 is fitted to a set of functions and the function coefficients are saved for use in simulations. Using the fit functions in a simulation is not only more portable but is also more than an order of magnitude faster than running Geant4. This model has been successfully incorporated into the *Bmad* simulation toolkit.

The output position, angular orientation, and momentum distribution is modeled. Preliminary support for modeling the polarization distribution is also discussed.

INTRODUCTION

A common method of producing positrons for use in an accelerator is through the use of a positron converter[1, 2]. This is typically a slab of heavy metal, such as tungsten, located in a Linac which is bombarded with electrons with energies of order 100 MeV. The electrons emit photons via bremsstrahlung which in turn decay to e^+e^- pairs via the reaction

$$e^- + Z \rightarrow e^- + Z + \gamma \rightarrow e^- + Z + e^- + e^+.$$

After the converter, the electrons and any other particles produced can be filtered off with a dipole magnet effectively "converting" a beam of incoming electrons into a beam of outgoing positrons.

Both bremsstrahlung from electrons traveling through the field of a nucleus and the subsequent e^+e^- pair production have been discussed at length in the literature[3–9]. Many of the theoretical treatments of bremsstrahlung and e^+e^- pair production are reviewed by Tsai[9]. Analytic expressions for both the bremsstrahlung radiation spectrum and secondary electron energy spectrum as functions of target thickness have been derived[3], and the problem has been treated across a wide range of incoming electron energies[4]. The bremsstrahlung cross section has been tabulated for a wide range of electron energies and target materials[5, 6]. Recently, computer codes have been developed to calculate the spectra and angular distributions of bremsstrahlung[7, 8], although these are designed to work at low energies (< 3 MeV).

Despite the extensive study of bremsstrahlung and pair production that exists in the literature, there is no closed

form description of the kinematics of positrons produced by bremsstrahlung from electrons impinging on a target. This problem has been treated numerically[10], but there is no existing machinery to incorporate these results into a full accelerator simulation. These prior efforts also do not address the production of polarized positrons from a beam of polarized electrons, a topic which is of current interest[11].

In response, the authors have developed a converter model and this model has been incorporated in the *Bmad* [12] accelerator toolkit. The model is designed to be flexible, accommodating any converter material and thickness as well as supporting arbitrary incoming and outgoing particle species. The model is also fast to use since the expensive physics calculations are performed only once when the converter model coefficients are being calculated. This is especially important when designing a machine with a converter as optimization simulations are typically time intensive.

One challenge in constructing the model was how to handle the complexity coming from the fact that the outgoing distribution has five dimensions (two spatial and three momentum) along with the incoming particle momentum, and orientation. Additionally, the target thickness and particle spin are potential degrees of freedom.

THE CONVERTER MODEL

The first step is to simulate the conversion process and calculate conversion probability coefficients. The coefficients can then be used to generate particles as part of a simulation of the machine the converter is a part of.

The coefficient calculation has two parts. The first part is to simulate the quantum electrodynamic[13] interactions of the incoming particles with the converter to produce bremsstrahlung photons and subsequent positrons. The distribution of the outgoing particles calculated in this first step is then used to calculate the coefficients for the expressions used to model the distribution.

Coordinate System

For concreteness, it will be assumed that the impinging beam is composed of electrons and the outgoing beam composed of positrons. The model itself is species agnostic.

Consider an electron incident on the upstream face of a positron converter of thickness T , with momentum p perpendicular to the face of the converter as depicted in Figure 1. The $(\mathbf{u}, \mathbf{v}, \mathbf{s})$ coordinate system (Figs. 1 and 2) is defined with \mathbf{s} perpendicular to the converter surface and the coordinate origin at the point where the electron would emerge if it was undeflected through the converter. Positrons produced in the converter emerge from the downstream face with some radial displacement r from the origin and at an angle θ relative to the \mathbf{u} axis as depicted in Figure 2. Define

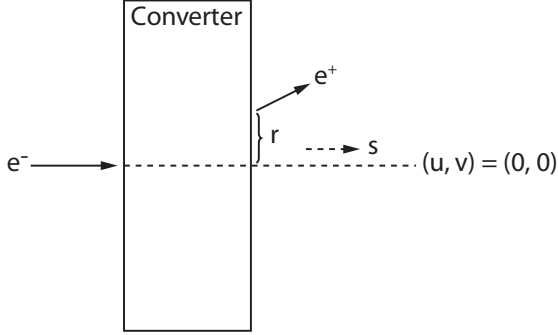


Figure 1: Positron converter coordinate system (side view).

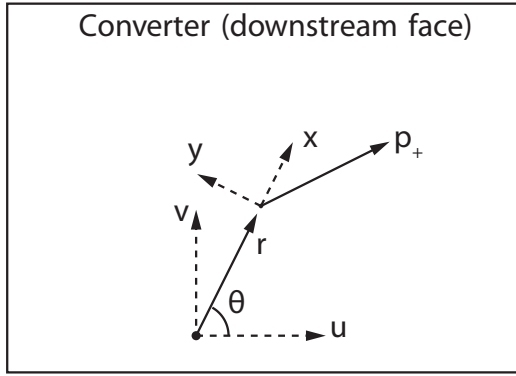


Figure 2: Positron converter coordinate system (view of the downstream face).

the rotated $(\mathbf{x}, \mathbf{y}, \mathbf{s})$ coordinate system so that \mathbf{x} is in the direction of \mathbf{r} .

By symmetry, θ must be uniformly distributed from 0 to 2π . The kinematic properties of the produced positrons which must be modeled are its radial displacement r and outgoing momentum \mathbf{p}_+ . The outgoing momentum is described in terms of its magnitude, p_+ , and the slopes along the \mathbf{x} and \mathbf{y} directions:

$$\frac{dx}{ds} = \frac{p_x}{p_s}, \quad \frac{dy}{ds} = \frac{p_y}{p_s} \quad (1)$$

Probability Distributions

At the downstream surface, positrons produced in the converter are described by the distribution

$$P\left(p_+, r, \frac{dx}{ds}, \frac{dy}{ds}; p_-, t\right), \quad (2)$$

P is the probability, per incoming electron, of producing an outgoing positron with momentum magnitude p_+ , radial displacement r , and momentum orientation $(dx/ds, dy/ds)$. P will have a dependence on the converter thickness t and incoming momentum p_- (non-normal incidence is discussed below). The converter thickness dependence is important if the converter thickness is allowed to vary in a simulation where the positron yield is to be maximized. To model the thickness and electron momentum dependence, the distribution P is calculated at a number of user defined thicknesses

t and electron momenta p_- . Interpolation is then used when generating particles with the model.

For a given t and p_- , the integral of P over the space $(p_+, r, dx/ds, dy/ds)$ will be the number of positrons n_+ produced per electron

$$\int P\left(p_+, r, \frac{dx}{ds}, \frac{dy}{ds}\right) dp_+ dr d\left(\frac{dx}{ds}\right) d\left(\frac{dy}{ds}\right) = n_+ \quad (3)$$

To simplify the computations, P is decomposed into two subdistributions,

$$P\left(p_+, r, \frac{dx}{ds}, \frac{dy}{ds}\right) = P_1(p_+, r) P_2\left(\frac{dx}{ds}, \frac{dy}{ds}; p_+, r\right) \quad (4)$$

where P_1 is the probability, per incident electron, of producing a positron with momentum magnitude p_+ and radial displacement r , and P_2 is the probability, for a given p_+ and r , of producing a positron with momentum orientation $(dx/ds, dy/ds)$. P_1 is normalized to n_+ and P_2 is normalized to one.

The P_1 probability distribution is characterized by a two dimensional lookup table that gives P_1 at specific values of p_+ and r . P_2 is approximated using a heuristically derived skewed Lorentzian distribution

$$P_2\left(\frac{dx}{ds}, \frac{dy}{ds}; p_+, r\right) = A \frac{1 + \beta \frac{dx}{ds}}{1 + \alpha_x^2 \left(\frac{dx}{ds} - c_x\right)^2 + \alpha_y^2 \left(\frac{dy}{ds}\right)^2} \quad (5)$$

where, as explained below, β , α_x , α_y and c_x will be characterized as functions of p_+ and r , and A is calculated from the normalization of P_2 .

To calculate coefficients, a program to simulate the passage of particles through matter is needed. This program was developed using the Geant4[14] particle physics library. A large number of electrons incident upon the converter are simulated and the produced positron distribution is recorded. From this, a fitting program is used to construct a two dimensional binned table of output probability P_1 as a function of p_+ and r . The user may specify values for p_+ and r to bin at or specify the desired number of bins in both dimensions to use. If the latter option is made, the fitting program will space the bins to give roughly equal number of particles in each bin. An example is shown in Figure 3. The probability of having a positron outside of the range of the table is taken to be zero. Inside the range of the table, the value of $P_1(p_+, r)$ is found by linear interpolation of the table data.

For the P_2 modeling, for each of the (p_+, r) bin points for P_1 , a least squares fit is made using Eq. 5 and the distribution of dx/ds and dy/ds for particles in the bin. Since the distribution in Equation 5 is not normalizable over the entire $(dx/ds, dy/ds)$ plane, as part of the fit, the fitting program calculates values for dx/ds_{\min} , dx/ds_{\max} , and $|dy/ds|_{\max}$, outside of which the value of P_2 is taken to be zero. These cuts are made so that P_2 covers 95% of the positrons generated by Geant4. The values of c_x , α_x , α_y , β , dx/ds_{\min} , dx/ds_{\max} , and $|dy/ds|_{\max}$ are obtained by a fit of the Geant4

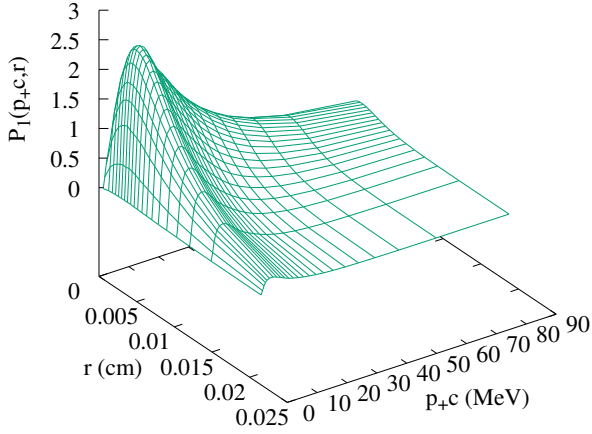


Figure 3: $P_1(p_+, r)$ for incoming electrons with $p_{-c} = 250$ MeV and a tungsten target of thickness $T = 6.35$ mm.

data in each (p_+, r) bin with the value of A fixed by the unit normalization of P_2 .

Once tables for the parameters c_x , α_x , etc. are calculated at the bin points, the tables are used for each of these parameters to fit the parameters as a function of p_+ and r . The fit for a given parameter is has two pieces. Above a user definable threshold in p_+ , a two dimensional fit in (p_+, r) is made of the form:

$$f(p_+)g(r) \exp(k_1 p_+ + k_2 r) + C \quad (6)$$

where $f(p_+)$ and $g(r)$ are third-order polynomials. Below the threshold, for each p_+ in the P_1 table, a 1D fourth-order polynomial fit in r is made. The 1D fits are performed for small values of p_+ because equation 6 tends to fit the Geant4 data poorly when $p_+ \lesssim 10$ MeV. Since most produced positrons are produced in this region, it is desirable for the P_2 parameter fits to be more detailed when p_+ is small.

Examples of the P_1 and P_2 distributions obtained from the Geant simulation are shown in Figures 3 and 4 respectively. The fit given in equation 5 models the data from Geant quite successfully, both when the parameters are obtained by direct fit to the data and when the parameters from the second order fits are used. The average χ^2 value for the direct fits is about 0.11, while the average χ^2 for the second order fits is about 0.14. The bins where the fit performs the worst have a χ^2 of about 1 for the direct fits, while the maximum χ^2 for the second order fits is about 2.2.

The Geant4 simulation and accompanying formalism assume that the incoming electrons are normally incident on the target. To adjust for a non-normal impinging electron when generating positrons with the converter model, the coordinate system is rotated so that the s axis is aligned along the incoming electron axis. The effective converter thickness used is adjusted to be $T \sec \phi$ where ϕ is the angle from the normal, as this is the distance from the electron beam's entry point on the converter's upstream face to its exit point

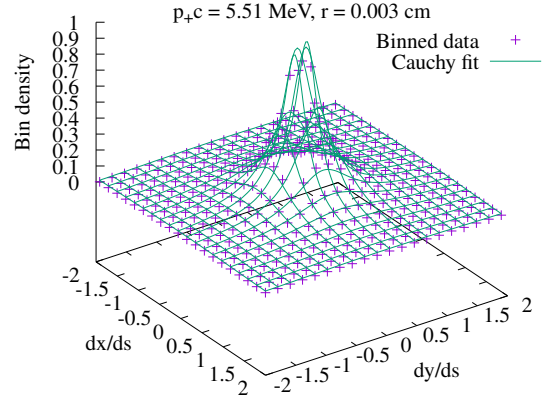


Figure 4: $P_2\left(\frac{dx}{ds}, \frac{dy}{ds}; p_+, r\right)$ for incoming electrons with $p_{-c} = 250$ MeV and a tungsten target of thickness $T = 6.35$ mm, and outgoing positrons with $p_{+c} = 5.15$ MeV and $r = 0.37$ mm. The purple points indicate data obtained directly from the Geant simulation, while the green curve shows the fit to the data.

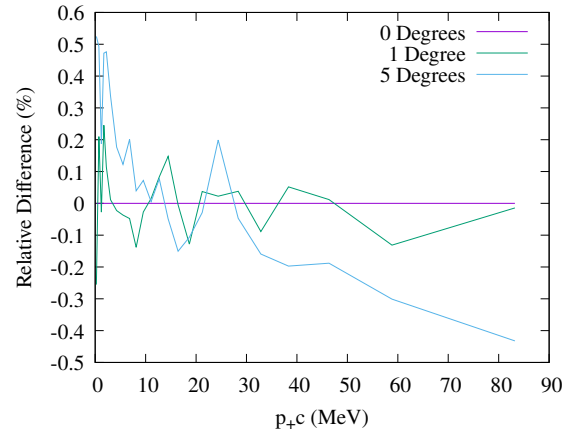


Figure 5: Relative discrepancy of the distributions of positron momenta for $\phi = 1$ and 5 degrees compared to the distribution for $\phi = 0$.

on the downstream face. The distributions of positron momentum p_+ , radial displacement r , and outgoing angle θ are shown in Figures 5-7 for various incoming angles ϕ . Up to 5 degrees off-normal there is very little deviation from the on-axis results. For a machine like the Cornell CESR Linac, where the impinging beam has an angular spread well less than 1 degree, the simple treatment of off-normal is a good approximation.

SPIN TRACKING

Polarization transfer from the incoming electrons to the outgoing positrons has also been modeled. Any incoming polarization \mathbf{S}_- may be specified, and histograms describing S_x , S_y , and S_z of the produced positrons as functions of

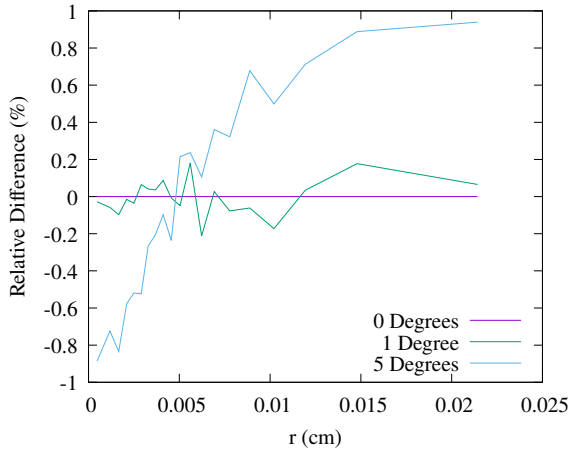


Figure 6: Relative discrepancy of the distributions of positron radial displacements r for $\phi = 1$ and 5 degrees compared to the distribution for $\phi = 0$.

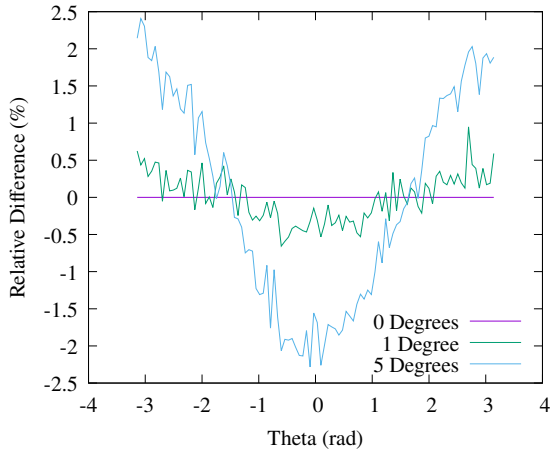


Figure 7: Relative discrepancy of the distributions of positron angle θ for $\phi = 1$ and 5 degrees compared to the distribution for $\phi = 0$.

p_+ and r are produced. In the Geant4 simulations done for this paper, it is observed that only the longitudinal polarization of the incoming electrons is ever transferred to the produced positrons; the produced positrons always have S_x and S_y essentially zero regardless of the incoming electron polarization.

Recently, the PEPPo collaboration[11] has published experimental results of polarized positron production from a polarized electron beam via bremsstrahlung, to which the spin tracking results from this simulation can be compared. This simulation yields polarization transfer efficiencies significantly higher than those observed experimentally for outgoing positrons with p_+c less than 5 MeV. In contrast, the simulation's results for higher momentum positrons agrees closely with experiment. The discrepancy is likely due to approximations made by the Geant4 library in computing polarization transfer during the pair production step. While this disagreement shows that the spin tracking components

of this simulation should not be relied on for accuracy at present, all of the infrastructure is in place to handle spin tracking. When more accurate spin tracking methods become available in Geant, this simulation, and the *Bmad* converter element, will be ready to use their results.

THE BMAD CONVERTER ELEMENT

Bmad is a software toolkit for the simulation of high energy charged particles and X-rays. To make use of the converter model, a converter element has been added to *Bmad* which uses the model coefficients as described above allowing for such things as a start to end simulation of the Cornell CESR Linac. The model coefficients are stored within a lattice input file which makes converter simulation portable to any *Bmad* based program.

For each incoming electron, *Bmad* randomly pulls values of p_+ , r , $\frac{dx}{ds}$, and $\frac{dy}{ds}$ from the interpolated probability distributions. Outgoing positrons are assigned a weighting factor proportional to the likelihood of producing a positron from the given incoming electron. This weighting factor is then used with any statistical analysis.

Agreement between direct output from Geant4 and emulated output from *Bmad* is quite good, with the distribution of particles from *Bmad* coming within a few percent of the Geant distributions. This is illustrated in Figure 8. *Bmad* simulates the positron converter approximately 20 times faster than the direct Geant4 physics simulations.

As the figure shows, the relative discrepancy between the distributions of positrons produced by Geant and *Bmad* agree within a few percent under most circumstances. The two scenarios where this is not the case are for the lowest energy bins, and for bins with large p_+ and large r . The discrepancy in the first case is due to the fact that *Bmad* does not produce positrons with p_+ below the value of p_+ used as the center of the first bin. This causes *Bmad* to produce less low-energy positrons than Geant. This discrepancy is acceptable, as virtually all of these low-energy positrons would be lost within a short distance from the converter. The discrepancy for large p_+ and r bins is also acceptable since very few positrons are produced in this region.

CONCLUSION

The converter model presented in this paper, when applied to positron production, provides simulation results that are in close agreement to Geant4's direct simulation of bremsstrahlung radiation and pair production. A small sacrifice in accuracy is made in return for a significant increase in simulation speed, making this method appropriate for use in lattice simulation and optimization software such as *Bmad*.

One of the primary motivators for this work was the desire to fully model the CESR linac lattice. Work is currently underway to use the model developed here. A first goal in this endeavor is to assess the agreement between the *Bmad* model of the linac as a whole the against the linac's experimentally observed beam. Once good agreement is established, *Bmad* can be used to optimize the lattice design, including

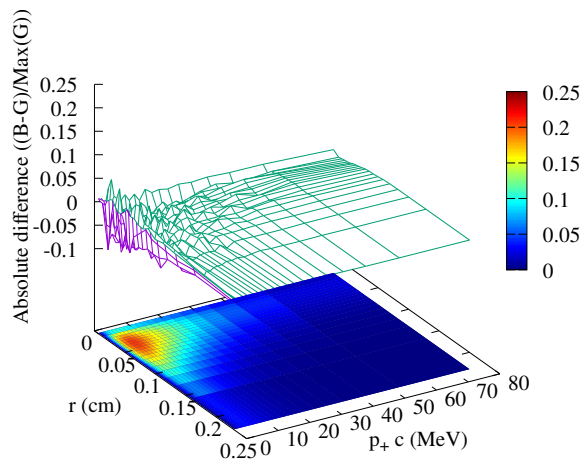


Figure 8: Comparison of the *Bmad* converter element with the Geant simulation. The surface plot shows the difference between the P_1 distributions generated by *Bmad* and by Geant, with the difference scaled by the maximum value of the P_1 distribution from Geant. The color plot shows the value of the P_1 distribution from Geant, indicating the region where obtaining accurate results from *Bmad* is most important.

quadrupole and solenoid tuning. Other future applications could include the optimization of element positioning on the linac beam line.

ACKNOWLEDGMENTS

Many thanks to Vardan Khachatryan for helping with running of Geant. This work is supported by National Science Foundation award number DMR-1829070.

REFERENCES

- [1] A. Mikhailichenko, “CESR’s Positron Source,” in *SLAC LC02*, Feb. 2002.
- [2] R. Andreani and A. Cattoni, “Positron converter for the Frascati linear accelerator,” *Nuclear Instruments and Methods*, vol. 129, no. 2, pp. 365–371, 1975, issn: 0029-554X. doi: [https://doi.org/10.1016/0029-554X\(75\)90726-0](https://doi.org/10.1016/0029-554X(75)90726-0). <https://www.sciencedirect.com/science/article/pii/0029554X75907260>
- [3] Y. S. Tsai and V. Whitis, “Thick-Target Bremsstrahlung and Target Considerations for Secondary-Particle Production by Electrons,” *Phys. Rev.*, vol. 149, pp. 1248–1257, 4 Sep. 1966. doi: [10.1103/PhysRev.149.1248](https://doi.org/10.1103/PhysRev.149.1248). <https://link.aps.org/doi/10.1103/PhysRev.149.1248>
- [4] H. K. Tseng and R. H. Pratt, “Exact Screened Calculations of Atomic-Field Bremsstrahlung,” *Phys. Rev. A*, vol. 3, pp. 100–115, 1 Jan. 1971. doi: [10.1103/PhysRevA.3.100](https://doi.org/10.1103/PhysRevA.3.100). <https://link.aps.org/doi/10.1103/PhysRevA.3.100>
- [5] S. M. Seltzer and M. J. Berger, “Bremsstrahlung spectra from electron interactions with screened atomic nuclei and orbital electrons,” *Nuclear Instruments and Methods in Physics Research Section B: Beam Interactions with Materials and Atoms*, vol. 12, no. 1, pp. 95–134, 1985, issn: 0168-583X. doi: [https://doi.org/10.1016/0168-583X\(85\)90707-4](https://doi.org/10.1016/0168-583X(85)90707-4). <https://www.sciencedirect.com/science/article/pii/0168583X85907074>
- [6] S. M. Seltzer and M. J. Berger, “Bremsstrahlung energy spectra from electrons with kinetic energy 1 keV–10 GeV incident on screened nuclei and orbital electrons of neutral atoms with $Z = 1–100$,” *Atomic Data and Nuclear Data Tables*, vol. 35, no. 3, pp. 345–418, 1986, issn: 0092-640X. doi: [https://doi.org/10.1016/0092-640X\(86\)90014-8](https://doi.org/10.1016/0092-640X(86)90014-8). <https://www.sciencedirect.com/science/article/pii/0092640X86900148>
- [7] A. Pořkus, “BREMS: A program for calculating spectra and angular distributions of bremsstrahlung at electron energies less than 3 MeV,” *Computer Physics Communications*, vol. 232, pp. 237–255, 2018, issn: 0010-4655. doi: <https://doi.org/10.1016/j.cpc.2018.04.030>. <https://www.sciencedirect.com/science/article/pii/S0010465518301462>
- [8] A. Pořkus, “Shape functions and singly differential cross sections of bremsstrahlung at electron energies from 10 eV to 3 MeV for $Z = 1–100$,” *Atomic Data and Nuclear Data Tables*, vol. 129-130, p. 101 277, 2019, issn: 0092-640X. doi: <https://doi.org/10.1016/j.adt.2019.03.002>. <https://www.sciencedirect.com/science/article/pii/S0092640X19300099>
- [9] Y. S. Tsai, “Pair production and bremsstrahlung of charged leptons,” *Rev. Mod. Phys.*, vol. 46, pp. 815–851, 4 Oct. 1974. doi: [10.1103/RevModPhys.46.815](https://doi.org/10.1103/RevModPhys.46.815). <https://link.aps.org/doi/10.1103/RevModPhys.46.815>
- [10] D. B. Fromowitz, “Increasing the positron capture efficiency of the CESR linac injector,” Ph.D. dissertation, Cornell University, Oct. 2000.
- [11] D. Abbott *et al.*, “Production of Highly Polarized Positrons Using Polarized Electrons at MeV Energies,” *Phys. Rev. Lett.*, vol. 116, p. 214 801, 21 May 2016. doi: [10.1103/PhysRevLett.116.214801](https://doi.org/10.1103/PhysRevLett.116.214801). <https://link.aps.org/doi/10.1103/PhysRevLett.116.214801>
- [12] D. Sagan, “Bmad: A relativistic charged particle simulation library,” *Nuc. Instrum. and Methods in Phys Research A*, vol. 558, pp. 356–359, 2006, <http://www.lepp.cornell.edu/~dcs/bmad>.
- [13] P. Zyla *et al.*, “Review of Particle Physics,” *PTEP*, vol. 2020, no. 8, sec. 34.4, p. 083C01, 2020. doi: [10.1093/ptep/ptaa104](https://doi.org/10.1093/ptep/ptaa104).
- [14] S. Agostinelli *et al.*, “Geant4—a simulation toolkit,” *Nuclear Instruments and Methods in Physics Research Section A: Accelerators, Spectrometers, Detectors and Associated Equipment*, vol. 506, no. 3, pp. 250–303, 2003, issn: 0168-9002. doi: [https://doi.org/10.1016/S0168-9002\(03\)01368-8](https://doi.org/10.1016/S0168-9002(03)01368-8). <http://www.sciencedirect.com/science/article/pii/S0168900203013688>